Science of the Total Environment 867 (2023) 161442

Contents lists available at ScienceDirect

Science of the Total Environment

journal homepage: www.elsevier.com/locate/scitotenv

Four-dimensional electrical resistivity imaging for monitoring pumping-induced saltwater intrusion in a coastal aquifer

Mark C. McDonnell [a,*], Raymond Flynn [a], Jesús Fernández Águila [a], Gerard A. Hamill [a], Shane Donohue [b], Eric M. Benner [a], Christopher Thomson [a], Georgios Etsias [a], Thomas S.L. Rowan [c], Paul B. Wilkinson [d], Philip I. Meldrum [d]

[a] Queen's University Belfast, School of Natural and Built Environment, Stranmillis Road, Belfast BT9 5AG, Northern Ireland, United Kingdom
[b] University College Dublin, School of Civil Engineering, Richview Newstead, Belfield, Dublin 4, Ireland
[c] Imperial College London, Civil and Environmental Engineering Department, London SW7 2AZ, England, United Kingdom
[d] British Geological Survey, Keyworth, Nottingham NG12 5GG, England, United Kingdom

HIGHLIGHTS

- Coastal water resource management key with population increase & sea level rise.
- Pumping test & novel geophysics tracked subsurface movements of saline interfaces.
- Intertidal saltwater cell can feed saltwater intrusion in coastal aquifers.
- Well design in coastal aquifers can be informed by geophysical methods.

GRAPHICAL ABSTRACT

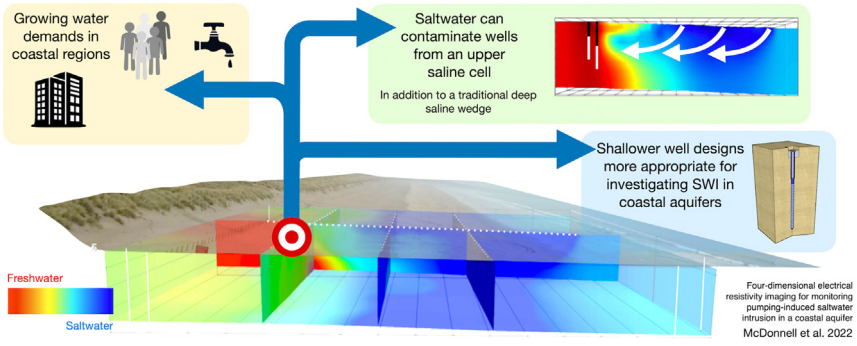

ARTICLE INFO

Editor: José Virgílio Cruz

Keywords:
Geophysics
Seawater intrusion
Pumping test
Coastal water resource management

ABSTRACT

Conventional views of saltwater intrusion (SWI), where a basal saline wedge extends inland below fresh groundwater, can be complicated by the influence of saltwater cells in the upper part of aquifers in areas affected by tidal cycles. Distinguishing the contribution of each saltwater source may prove fundamental for well design and resource management. Application of time-lapse electrical resistivity imaging (ERI) during a 32-h pumping test in a pristine unconfined coastal sand aquifer, affected by strong tidal ranges (>2 m), aimed to evaluate the potential of the method to characterize the source of induced SWI in four dimensions (three dimensions and time). Water level monitoring during the test revealed that at the end of pumping, the upper 2 m of the aquifer had dewatered in the vicinity of the well field, reversing hydraulic gradients between the aquifer and the sea. This induced SI, with mixing models of well head water quality suggesting that saline water contributions to total discharge rose from 4 % to 8 %. ERI results reflected dewatering through an increase in resistivity in the upper 2-6 m of the aquifer, while a decline in resistivity, relative to background conditions, occurred immediately below this, reflecting the migration of saline water through the upper layers of the aquifer to the pumping well. By contrast no change in resistivity occurred at depth, indicating no significant change in contribution from the basal saline water to discharge. Test findings suggest that future water resource development at the site should focus on close monitoring of shallow pumping, or pumping from deeper parts of the aquifer, while more generally demonstrating the value of time-lapse geophysical methods in informing coastal water resource management.

* Corresponding author.
E-mail address: mmcdonnell23@qub.ac.uk (M.C. McDonnell).

http://dx.doi.org/10.1016/j.scitotenv.2023.161442
Received 30 September 2022; Received in revised form 8 December 2022; Accepted 3 January 2023
Available online 6 January 2023

1. Introduction

Saltwater intrusion (SWI) in coastal aquifers is a well-documented phenomenon, occurring in many parts of the world. Werner et al. (2013) provides a detailed description of the issue and the challenges it poses, noting that SWI can occur when coastal aquifers are over-pumped for freshwater, drawing saltwater into wells. The arrival of saline water in a pumping well can render it incapable of supplying potable water for considerable periods. Typically, deeper wells are considered more susceptible to this process since the denser saltwater can naturally extend inland at depth in the form of a deep saltwater wedge (DSW). In coastal aquifers affected by tidal cycles, apart from the DSW at the base of an aquifer, an intertidal saltwater cell (ISC) in the upper part of the aquifer can also exist. This forms in the intertidal zone of unconfined coastal aquifers when seawater infiltrates into the top of the aquifer. Contributing factors to the configuration of both the DSW and the ISC include the amount of aquifer recharge, coastal topography and aquifer (geological) heterogeneity, while the size of the ISC can vary depending on the tidal amplitude (Cardenas et al., 2015; Maury and Balaji, 2015). Consequently, coastal aquifers exhibiting an ISC may experience saltwater contamination derived from the top of the aquifer. This has impacts for coastal water supply design, potentially rendering traditional shallow-wells inappropriate. The focus of this paper investigates the potential of continuing to use these wells under close monitoring.

Electrical resistivity imaging (ERI) is a popular geophysical technique often used to detect and monitor subsurface phenomena based on differences in their electrical properties, without physically penetrating the ground surface. While ERI is a popular technique for surface investigations (Loke and Barker, 1996; Barker and Moore, 1998), it has been relatively underutilized in monitoring aquifer responses to pumping tests compared to ground penetrating radar (Endres et al., 2000; Bevan et al., 2003), or self-potential techniques (Rizzo et al., 2004; Straface et al., 2007). Nonetheless, (Barker and Moore (1998), and, subsequent work by Chang et al. (2017), successfully used ERI to monitor saturation changes and estimate general hydraulic properties in unconfined aquifers during pumping tests. Overall, however, the number of studies which have used ERI during pumping tests remains small. ERI proves an especially useful tool in the characterization of saltwater patterns due to the contrast in resistivity between saltwater and freshwater (Hermans and Paepen, 2020). Several studies suggest that indirect methods such as ERI have the potential to supersede more expensive direct investigation methods (Land et al., 2004; Zarroca et al., 2011). However while ERI could prove effective at characterizing saltwater movements in an aquifer, it can only provide an indication of subsurface conditions directly below the area of investigation; this contrasts with chemical analyzes, for example, which can provide evidence for the source of groundwater at greater distances from the immediate area of investigation (Bear et al., 1999).

The development of automated acquisition of ERI data (Loke and Barker, 1995; Pidlisecky et al., 2007; Pidlisecky and Knight, 2008) and more recently, time-lapse inversions (Johnson et al., 2010; Legaz et al., 2009; Müller et al., 2010; Pollock and Cirpka, 2012) — especially in purpose-built monitoring instrumentation with telemetric control, data transfer, scheduling and processing — have enabled higher-frequency and longer-term geophysical monitoring in several settings (LaBrecque et al., 2004; Ogilvy et al., 2009; Chambers et al., 2014; Uhlemann et al., 2017; Holmes et al., 2022). Moreover, this approach has the ability to perform differential resistivity imaging, where the resistivity values from one time snapshot are subtracted from another to produce the change in resistivity with time (Chang et al., 2017). This approach overcomes the complications associated with confident interpretation of resistivity responses due to geological heterogeneity. One such recent example of an automated, four-dimensional (time-lapse, 3D) ground resistivity imaging system is *PRIME*, a product of research at the British Geological Survey which supports remote installation, low power consumption and low cost (Holmes et al., 2020). Despite the benefits of time-lapse ERI, it remains relatively underutilized in the investigation of induced SWI. One such reason is that confident data interpretation can be complicated by external disturbances arising from groundwater exploitation from multiple sources. This approach displays considerable potential to consistently monitor induced saline intrusion over prolonged periods.

This paper reports on geophysical investigations monitoring response to experimentally induced SWI in a relatively homogenous, unconfined coastal aquifer, affected by tidal cycles, using four-dimensional ERI. The absence of additional abstractions in the investigation area selected has facilitated more confident interpretation of research findings. Investigations form part of a wider multidisciplinary study in which geophysical data collection has been complimented by hydraulic measurements and water quality sampling/monitoring to permit the source of salt water entering pumping wells to be identified. In bringing together two important spheres of hydrogeological research – aquifer responses to pumping, and tidal impacts on coastal aquifers – this study represents the first time that ERI has been applied to monitoring the response of a pumping test in the intertidal zone of a coastal aquifer. The wider implications of this study lie in the supply of water to vulnerable coastal communities, as water resources become increasingly stressed. Studies of this nature are at the nexus of anthropogenic requirements of coastal aquifers and the need for a deeper understanding of tidal processes within coastal aquifers, which have heretofore been studied almost exclusively through modeling efforts.

2. Material and methods

2.1. Site description

To test the hypothesis that four-dimensional ERI can be employed to monitor and detect saltwater interfaces under pumping, a well field was installed in coastal sands, unaffected by groundwater abstraction. A beach on the Magilligan Peninsula in County Derry, Northern Ireland (Magilligan) was selected for this purpose Fig. 1A). The site has been described in detail in previous studies (Carter, 1975; Robins and Wilson, 2017; Águila et al., 2022). Twenty metres of relatively homogenous, fine-medium grained Holocene sands underlain by low permeability Lower Jurassic Mudstone (McCann, 1988) occur adjacent to an intertidal zone up to 100 m wide (Pingree and Griffiths, 1981). The area experiences direct recharge of 400 mm/year via precipitation, with no overland flow or groundwater throughflow (Robins and Wilson, 2017). Magilligan has proven particularly suitable to study SWI due to prevalence of beach sand deposits encountered in other parts of the world. Moreover, low levels of aquifer heterogeneity encountered at the site permit interpretation of geophysical data with greater confidence.

Águila et al. (2022) used the combination of geophysical and geotechnical methods, along with groundwater sampling, to characterize the Magilligan aquifer in detail. Results from that study reveal low levels of aquifer heterogeneity below the site. Critically, preliminary ERI measurements completed in the study area revealed the presence of an upper, low-resistivity lens (< 3Ωm), which, at its deepest, is over 8 m thick in the vicinity of the tidal low water mark, overlying a higher resistivity unit. Cone penetrometer testing (CPT) and associated high-resolution hydraulic profiling, coupled with water quality sampling, revealed the lens to reflect an ISC, which restricted freshwater discharge from a relatively homogeneous sand unit to a zone of seepage of less-saline water, seaward of the ISC.

To facilitate site-scale experimentally induced SWI into that part of the sands containing freshwater, a suite of pumping and observation wells were installed above the mean high tide mark. Fig. 1D summarizes the location, function (pumping or observation) and depth of each well, while Table 1 summarizes screened depths, diameters, and coordinates. Briefly, the well array comprised three pumping wells; one seaward well, installed to ten metres below ground surface (mBGS) (Pw1); and a further two landward pumping wells, installed to eight mBGS (Pw2 and Pw3) aimed to intercept landward freshwater contributions from the dune system to the south, otherwise flowing to Pw1. Three monitoring well clusters, installed in front of, behind and to the side of Pw1 consisted of four separate monitoring wells installed to depths of two, four, six and eight metres. All wells were

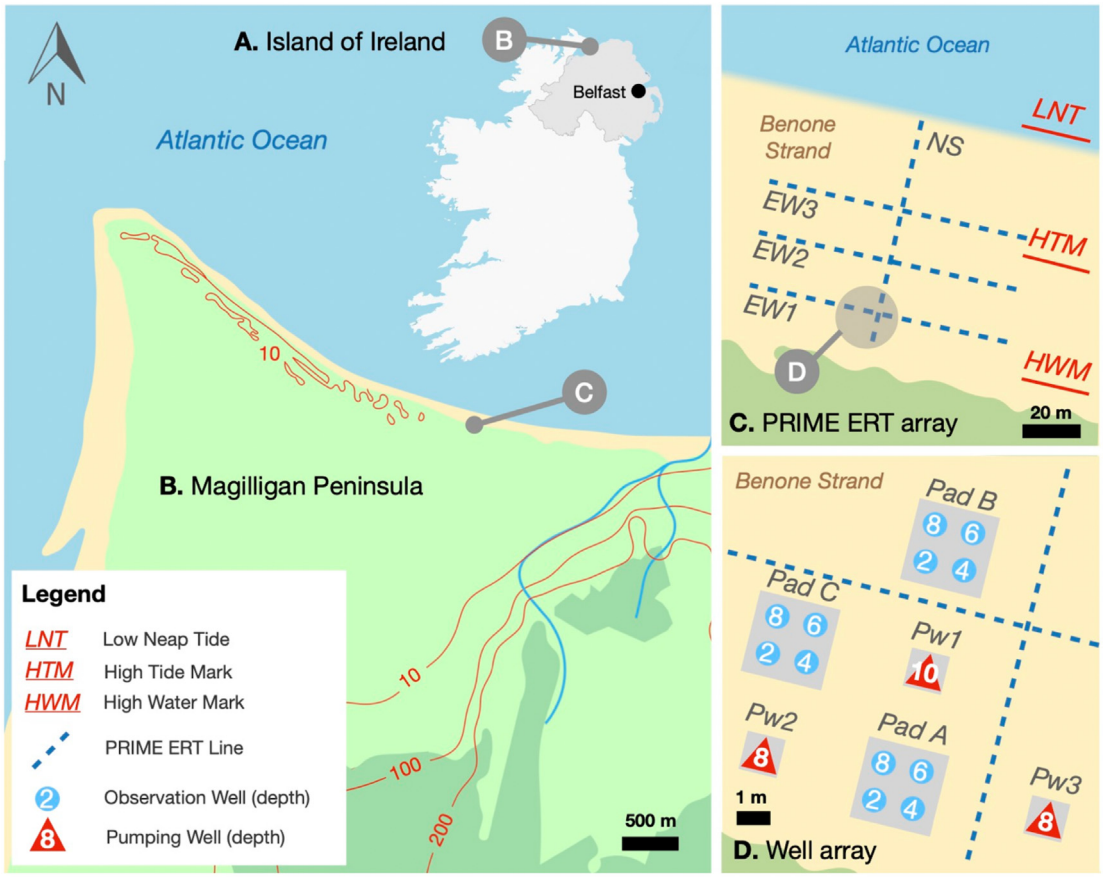

Fig. 1. A. Location of the Magilligan test site. **B.** Detail of the Magilligan Peninsula with topography. **C.** The four *PRIME* Electrical Resistivity Imaging lines and tide markers within the intertidal zone: low neap tide (LNT), high tide mark (HTM) and high water mark (HWM). **D.** The well array and *PRIME* ERI lines.

constructed using PVC casing and screen, with five-millimetre screen slots covered by a 300 μm geotextile.

2.2. Pumping test

A constant-rate pumping test involving the simultaneous pumping of all three pumping wells, was conducted to experimentally induce intrusion of salt water into that part of the sands containing freshwater. Testing was conducted during a transitional phase of the tidal cycle (between Spring and Neap tides) to provide the best tidal conditions under which SWI could be induced, while enabling unimpeded access to all wells throughout.

Table 1
Properties of wells installed at the Magilligan test site.

Well ID	Diameter (mm)	Purpose	Screened Depth (metres b.g.s.)	Latitude	Longitude
Pw1	150	Pumping	5–10	55.169231	−6.884934
Pw2	150	Pumping	5–8	55.169203	−6.885058
Pw3	150	Pumping	5–8	55.169226	−6.885051
A2	100	Observation	1–2	55.169184	−6.885005
A4	100	Observation	3–4	55.169182	−6.885008
A6	100	Observation	5–6	55.169185	−6.885013
A8	100	Observation	7–8	55.169187	−6.885017
B2	100	Observation	1–2	55.169378	−6.884951
B4	100	Observation	3–4	55.169372	−6.884953
B6	100	Observation	5–6	55.169374	−6.884964
B8	100	Observation	7–8	55.169372	−6.884968
C2	100	Observation	1–2	55.169257	−6.885072
C4	100	Observation	3–4	55.169251	−6.885071
C6	100	Observation	5–6	55.169254	−6.885087
C8	100	Observation	7–8	55.169252	−6.885084

Caprari 98 mm borehole electrical submersible pumps (Modena, Italy) with non-return vales, installed in each of the pumping wells, discharged water at a fixed rate over a 32-h period. Headworks for all pumps comprised a flowmeter (*B Meters GMDM-I*) placed 1.5 m from the top of the pump riser followed by a valve installed 1.5 m down-flow of the meter to permit fine tuning of discharge rates, while a 13 mm outlet tap was also fitted immediately upstream to enable water quality sampling. Pumping rates were set at 2.8 L/s in Pw1, and 3 L/s in both Pw2 and Pw3. The discharge water from pumping was conveyed via surface hoses to the intertidal zone at a point approximately 80 m along the shore, beyond the extremities of the ERI lines (Fig. 1C). Preliminary groundwater modeling suggested that this point lay outside of the zone of contribution for the well field thus preventing recirculation of pumped water within the aquifer, and potential impacts on geophysical signals.

A *YSI Pro Plus* multiparameter water quality meter with flow cell, fitted to the 13-mm outlet tap on the outflow from each pumping well, permitted semi-continuous measurement (10-min intervals) of discharge specific electrical conductance (SEC), water temperature, dissolved oxygen (DO) and oxidation reduction potential (ORP) over the duration of pumping. Calibration of the instrument using standard solutions took place immediately before the first measurement was taken. Additionally, the sampling tap permitted water sample collection for laboratory analysis at three-hour intervals throughout pumping, with eleven samples collected during the test. Samples were refrigerated in a dark location immediately after collection and submitted for major ion analysis (Na, K, Ca, Mg, SO4, Cl and alkalinity) within 24 h of collection.

Automated groundwater level measurements were taken at 60-s intervals using *Solinst LTC Edge* Leveloggers (Georgetown, Canada), and manually monitored at regular intervals throughout testing for

validation. Groundwater level monitoring began 17-h before pumping, and continued throughout pumping, until 13-h after the end of pumping.

2.3. Geophysical investigations

ERI was employed to track the migration of saltwater associated with pumping, and to quantify the effect that SI had on the sand resistivities. Electrode configuration at Magilligan comprised four lines of 32 stainless steel rods (128 electrodes in total), spaced at 2 m intervals in the case of the North-South (NS) profile, and at 2.5 m intervals in the case of the three East-West (EW) profiles (Fig. 1C). These were connected to a *PRIME* system which took electrical resistivity measurements at set time intervals and sent the data to a remote server via a mobile Internet connection. These allowed subsurface conditions to be monitored continually through time to develop a four-dimensional (4D) ERT dataset. The full three-dimensional array was positioned between the low-neap-tide and high water mark (HWM), where the ISC was suspected to prove most prominent.

The tops of all electrodes were installed at 0.5 m below ground surface to reduce the likelihood of electrodes becoming exposed during a high-energy tidal event. This also serves to improve contact resistance values by ensuring that the electrodes are closer to the water table. These locations, and the beach topography, were recorded using a *Leica Gs08* differential GPS (dGPS), attaining 2 mm XYZ accuracy. A profile of the topography of the beach surface was also taken with the dGPS to determine the depth at which the electrodes were placed.

The degree of change in resistivity which occurs during a full cycle under passive hydraulic gradients must be ascertained to confidently identify changes in resistivity that are due to pumping. Abarca et al. (2013) reported that the ISC undergoes its full degree of change over the course of one lunar cycle (approximately 28 days), growing in size after the neap tides of the First Quarter moon, reaching its maximum size with the New Moon and waning again by the First Quarter neap tide. In the present study, ERI snapshots were captured regularly throughout one tidal cycle, beginning at the First Quarter moon (neap tide) on 30th August 2021 and ending at the next First Quarter neap tide on 29th September 2021 (Fig. 2A). The *PRIME* system was installed, calibrated, and validated with other ERI instruments in the months prior to the pumping test, allowing reliable background monitoring to take place both during and after the pumping test. Conducting background monitoring almost six months after pumping ensured that there were no residual transient effects in the sands due to pumping. To capture the changes in resistivity due to pumping, high-frequency ERI measurements were taken for a period several hours before, during, and for several hours after pumping. The pumping monitoring regime took place between 11th and 13th May 2021, while the longer-term background monitoring took place between 16th May and 14th June 2021 (Fig. 2B). A complete ERI snapshot took approximately 60 min to collect. Tidal data were recorded at 15-min intervals at the closest monitoring station (Portrush harbour; 15 km east). The 3D inversion software used to analyze the data, Res3DInv from *Geotomo Software* (Loke, 2017), limited the maximum number of sequential 4-D snapshots to 25. For the background monitoring, snapshots were spaced as evenly as possible throughout the tidal cycle. During the pumping phase of data collection, measurements were taken on average every 5 h before, during and after pumping. This interval facilitated data collection by other, passive geophysical measurements (not considered in this study). The ERI system made use of a Dipole-Dipole array since this type of array is effective in mapping both vertical structures and exhibits better horizontal data coverage than some other array types (Loke, 2022). Two baseline ERI profiles were taken 10.35 h and 4.35 h before pumping began. The former was used to reference any changes in resistivity which occurred during pumping. Additionally, to capture recovery due to pumping, ERI profiles were taken at 4.5, 9 and 15 h after pumping stopped. Results reveal a maximum penetration depth of 14 m below ground surface.

ERI data were inverted using an iteratively reweighted Gauss–Newton least-squares method with an L1 norm on the data misfit, an L1 spatial smoothness constraint, and an L2 temporal smoothness constraint, which

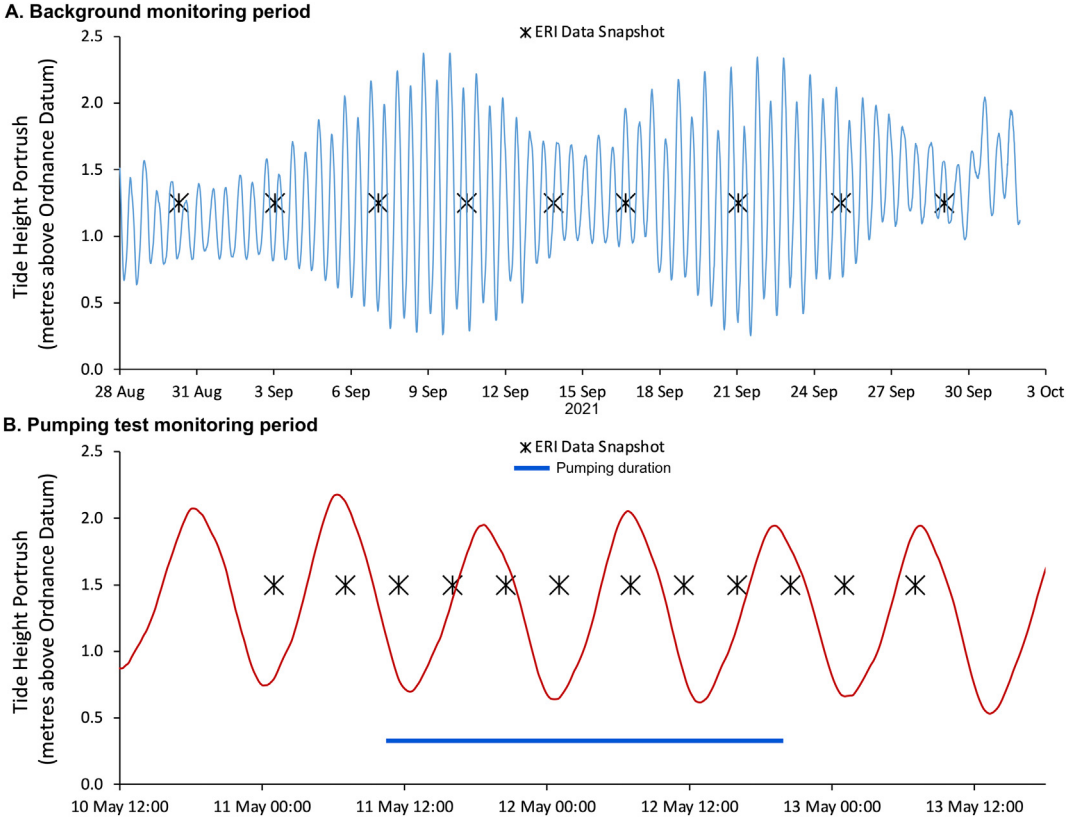

Fig. 2. Graph displaying the times when ERI snapshot profiles were taken as part of background monitoring phase (**A**) and during the pumping test (**B**) at the Magilligan test site with respect to tides.

ensures that changes vary smoothy with time (Loke, 2017). This difference, given by the RMS error (root-mean-squared error), and the model iteration selected as the best model, corresponds to the model in which the RMS error undergoes very little change (2–5 %) from one model iteration to the next. The data for all four lines of electrodes were inverted together to produce a sequence of output files which were displayed in *ParaView*™ (Avachit, 2015).

To enable comparison between pumped water resistivity and bulk electrical resistivity measurements acquired by the ERI (ρr), the SEC of the pumped groundwater (ρf) was converted to ρr using Archie's law (Archie, 1942):

$$\rho r = a\rho f\varphi - m$$

where a is a parameter related to the tortuosity, φ is the porosity and m is the cementation factor. a and m are constants, for which values of $a = 1$ and $m = 1.3$ were used due to the unconsolidated nature of the ground medium (Archie, 1942). The porosity of the sands at Magilligan has been determined at 0.35 (Águila et al., 2022), but since that study acknowledges some difficulties in taking representative samples without disturbing the loosely packed grains and the lack of sand samples at depth, this study uses porosities of 0.25 (coarse sand) and 0.45 (fine sands) to constrain ρr minimum and maximum values (Freeze and Cherry, 1979).

3. Results

3.1. Pumping test

Throughout pumping, the flow rate from all three pumping wells was maintained at constant rate of approximately 3 L/s for the 32-h test. Comparison between observation wells reveals that those areas more distal from the region of pumping (especially Pad B), experienced less drawdown than those closer to the area of abstraction. At the end of pumping, well A8, which is within 3 m of both Pw1 and Pw2, experiences a drawdown of 2.16 m, while well B6, which is over 5 m away from only Pw1, experiences a maximum drawdown of 1.44 m. Fig. 3A indicates that drawdowns reached up to 2 m in the observation wells by the end of pumping. The selection of observation well responses presented all show comparable trends of drawdown with time. The trend observed in pumping wells differed from those in the observation wells, with a sharper initial decrease in water level, which stabilized toward the end of the test. A sharper initial recovery is also exhibited in the pumping wells. All three pumping wells exhibit a similar trend of with time. Full recovery did not occur during the post pumping monitoring period (13h). However, extrapolation of observation well data suggests that full level recovery would take 46 h following the cessation of pumping (Fig. 3A). By contrast, the standard deviation of the water levels in each well in the five days preceding the pumping test is shown in Table 2. This reveals that under natural conditions, these wells exhibit an average of 4 cm change rise and fall in water level. Accordingly, the well levels recorded during the pumping test are representative of the effect of pumping and not natural factors (such as tides). The drawdown data in Fig. 3 also suggest that tides have a negligible effect on the dewatering process.

3.2. Water chemistry

The Durov plot, presented in Fig. 4, summarizes the change in major ion chemistry in pumping well discharges as pumping proceeded. Although samples collected from the landward wells display a stronger CaHCO3 signature, water from all three pumping wells displayed consistent increases in the relative proportions of sodium and chloride, with the relative importance of calcium and bicarbonate declining. This shift is most pronounced in Pw1. In Pw1, Na values increase from 87 mg/L to 222 mg/L at the end of pumping, while Cl values increase from 196 mg/L to 567 mg/L by the end of pumping. The respective changes for Pw2 are 22 mg/L and 37 mg/L, and for Pw3 are 31 mg/L and 41 mg/L. The changes and increases in major ion concentration proved consistent with the increases in well head SEC observed.

3.3. Well head water quality

Water quality measurements taken at the well head and presented in Fig. 3C, shows that Pw1 exhibits the greatest change in conductivity, rising from 1200 μS/cm at the start of pumping to a maximum of 2300 μS/cm at the end. Greater conductivity values indicate more saline water was drawn into the pumping wells during the test, although the trend proves variable. Conductivity initially declines in the well, reaching a minimum value of around 900 μS/cm after around 4 h of pumping, before subsequently rising to exceed concentrations observed at the start of pumping. This trend continues until the end of the test. Pw2 and Pw3 express more subtle variations in conductivity during pumping but exhibit an overall trend comparable to that of Pw1, with changes of 160 μS/cm and 50 μS/cm respectively. Fig. 3D presents dissolved oxygen (DO) concentrations measured in the discharge water from all three pumping wells. Pw1 and Pw3 exhibit a steady rise in DO, similar to their SEC patterns, but do not exhibit any large, sharp increases in DO.

3.4. Geophysical data

Fig. 5A presents a resistivity profile of the *PRIME* array determined from data collected 10 h before the beginning of pumping, representing the natural condition of the site in terms of resistivity immediately before pumping. Data suggest sands had higher resistivity on the landward side of the profile, becoming more conductive moving seawards. It is noteworthy that an area of lower resistivity (20–30 Ω.m) is present at the surface of the north-south profile, beginning at 15 m from the profile origin and extending seawards, with progressively increasing depth. Resistivity values below this area are higher, particularly evident between 15 and 25 m from the profile origin (140 Ω.m) (see Supplementary Video 1 for an animation of resistivity variations during pumping).

A comparison between the resistivity of the discharge water from the three pumping wells with the resistivity of the area around abstraction is shown in Fig. 6. Discharge water conductivity is converted to bulk resistivity (using a range of porosities) for comparison with ERI data (as described in Section 2.2). The ERI data were extracted from the *PRIME* model block within which the screened section of Pw1 fell. This block was approximately $2m^3$ in size and corresponded with the central section of the 5 m-long well screens. The bulk resistivity data within each block were interpolated by the inversion software. In Pw1, the results from the two data sources exhibit a similar trend with similar values. In Pw1, the bulk resistivity at the beginning of pumping was around 70 Ω.m and declined to around 30 Ω.m by the end of pumping. The bulk resistivity values from the PRIME model correspond slightly less well with the respective discharge water resistivity in Pw2 and Pw3, remaining mostly within the range calculated using Archie's Law, although the values in Pw2 deviate outside this range after 9 h of pumping. Fig. 5A indicates that the lowest bulk resistivity in the area surveyed has a resistivity of 1 Ω.m. All values from the *PRIME* model lie within the range calculated via Archie's Law.

The pattern of resistivity increases initially around the screened interval of Pw1, before steadily decreasing until plateauing after around 27 h of pumping. Pw2 and Pw3 exhibit less change in resistivity over the course of pumping. The resistivity trend measured with the *PRIME* system do not correspond as well with the discharge water in the interceptor wells, especially so in Pw2.

Fig. 5B highlights natural changes in water resistivity that occurred over the course of a full lunar cycle. There is a net decrease in resistivity in the upper 4 m of the sands, particularly between 10 m and 40 m north of the HWM, while there is a net increase in resistivity at depths below 4 m from the surface, between 20 m and 50 m north of the HWM. This trend is expressed relatively evenly in the east-west direction (parallel with the coastline). There are diffuse patches of positive and negative changes in resistivity at the seaward extremity of the profile, while the landward section

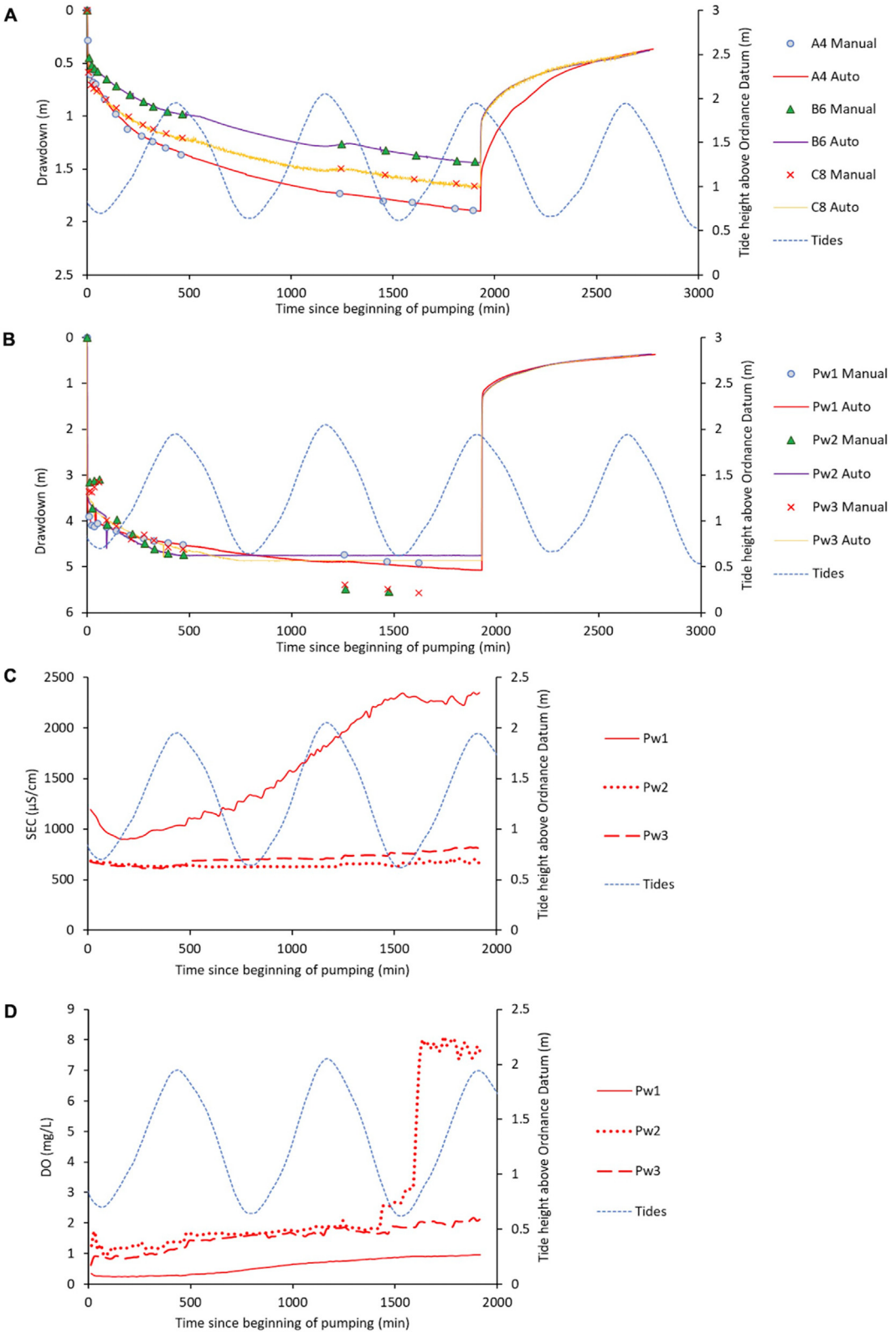

Fig. 3. Plots displaying the measured drawdown (manual and automated measurements) effected by pumping in observation wells A4, B6 and C8 (**A**); and in pumping wells (Pw) 1,2 and 3 (**B**) with respect to tides (note: after approximately 10 h of pumping, the water levels fell below the level of the logging instruments in Pw2 and Pw3 resulting in unreliable data); and the specific electrical conductance (SEC) (**C**) and dissolved oxygen (DO) (**D**) measured from the pumped water during the pumping test at the Magilligan test site with respect to tides.

(around the pumping wells) exhibits almost no change in resistivity over a full tidal cycle (see Supplementary Video 2 for an animation of resistivity variations during a tidal cycle).

The areas expressing change in resistivity under pumping are represented in Fig. 7. Snapshots reveal that the area around the well screens expresses the greatest degree of change, while those near the surface around

Table 2
Standard deviation (σ) in water levels recorded in observation wells via automatic loggers in the five days prior to pumping (the pumping wells and wells B8 and C8 were not equipped with logging instruments in the days prior to the pumping test); and the final drawdown measurements in each well immediately before pumping stopped.

Well ID	Standard deviation in natural well water level 05/05/21–10/05/21 (m)	Final drawdown at end of pumping test (m below top of well casing)
Pw1	–	4.92
Pw2	–	5.54
Pw3	–	5.58
A2	0.033	*Well was dry at the end of the pumping test*
A4	0.034	1.89
A6	0.037	2.15
A8	0.038	2.16
B2	0.046	1.51
B4	0.046	1.57
B6	0.051	1.44
B8	–	1.43
C2	0.044	1.62
C4	0.043	1.83
C6	0.044	1.79
C8	–	1.66
Average σ:	**0.042**	

the pumps express an overall increase in resistivity. The size of the areas expressing change gradually increase with pumping. After the cessation of pumping, their size begins to decrease again. The maximum discernible extent of dewatering just before pumping stopped is marked in Fig. 7E.

Comparing the background changes in resistivity with those experienced during pumping, the pattern of change is quite different. The area around the intersection of the north-south profile and the most landward east-west profile (EW1) experiences a reversal in resistivity, with the pumping test effecting a decrease in resistivity in this region, compared to the natural cycle which expresses an increase in resistivity in this region through a tidal cycle. While under natural conditions, there is a small amount of increase in resistivity near the surface during a tidal cycle in this region, under pumping, there is a further increase in resistivity, and in a more concentrated area above the pumping wells. There is no apparent change in resistivity in the deeper layers of the area surveyed, in either the background or the pumping scenario.

Three snapshots from the NS profile are shown in Fig. 8, the first from immediately before the beginning of pumping, the second from the end of pumping and the third from 15 h after pumping stopped. These snapshots reveal the change experienced in resistivity after pumping and then how the beach sands recovered after pumping stopped. The NS profile was selected because it best highlights the changes in resistivity that occurred during pumping with respect to the source of the water (i.e., from the ISC, or from the DSW), while also showing clearly the area immediately above the wells where pumping-induced dewatering would be expected to occur – i.e. the areas of deeper red and yellow at the surface above the pumping wells. An area of lower resistivity water intruded toward the pumping wells at around 4 m below ground level and persisted 15 h after pumping. The area between 7 m and 15 m from the southern end of the profile refilled with water of lower resistivity (8-15 Ω.m), which contrasts with the resistivity of the area pre-pumping — c. 50 Ω.m.

4. Discussion

Background monitoring at the Magilligan Test Site reveals that under natural conditions, the site experiences little variation in the water table, with fluctuations of on average 4 cm over the 5 days immediately prior to pumping. By contrast, under pumping, the water level in the observation wells dropped by an average of 1.7 m (Table 2). With regards to resistivity, as shown in Fig. 5B, during a full lunar/tidal cycle, there is a vertical contrast between the upper 4 m of the sands and the lower. The shallower depths exhibited negative changes in resistivity, corresponding to an increase in salinity, while below this, there was a decrease in salinity. These areas are likely to be the ISC, increasing in size in the shallower areas, and decreasing in the deeper areas. The east-west consistency of the trend supports the point that this is the ISC, since this feature would be expected to behave in a consistent manner along the coastline. These changes are consistent with the waxing and waning of the ISC through a tidal cycle, as

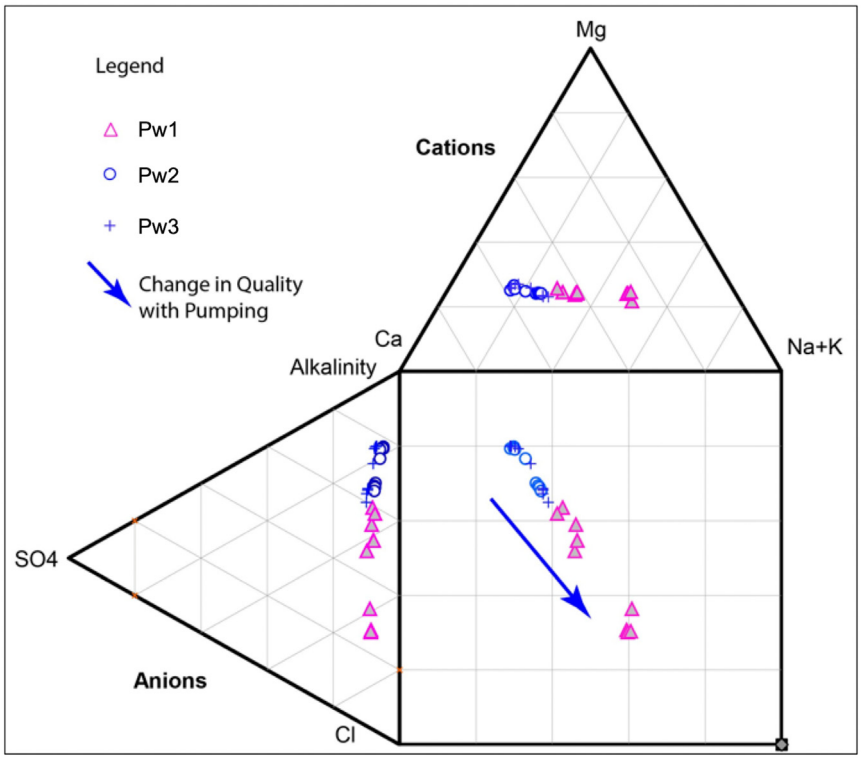

Fig. 4. Durov plot displaying the change in concentration of major ions in pumped water during the pumping test at the Magilligan test site.

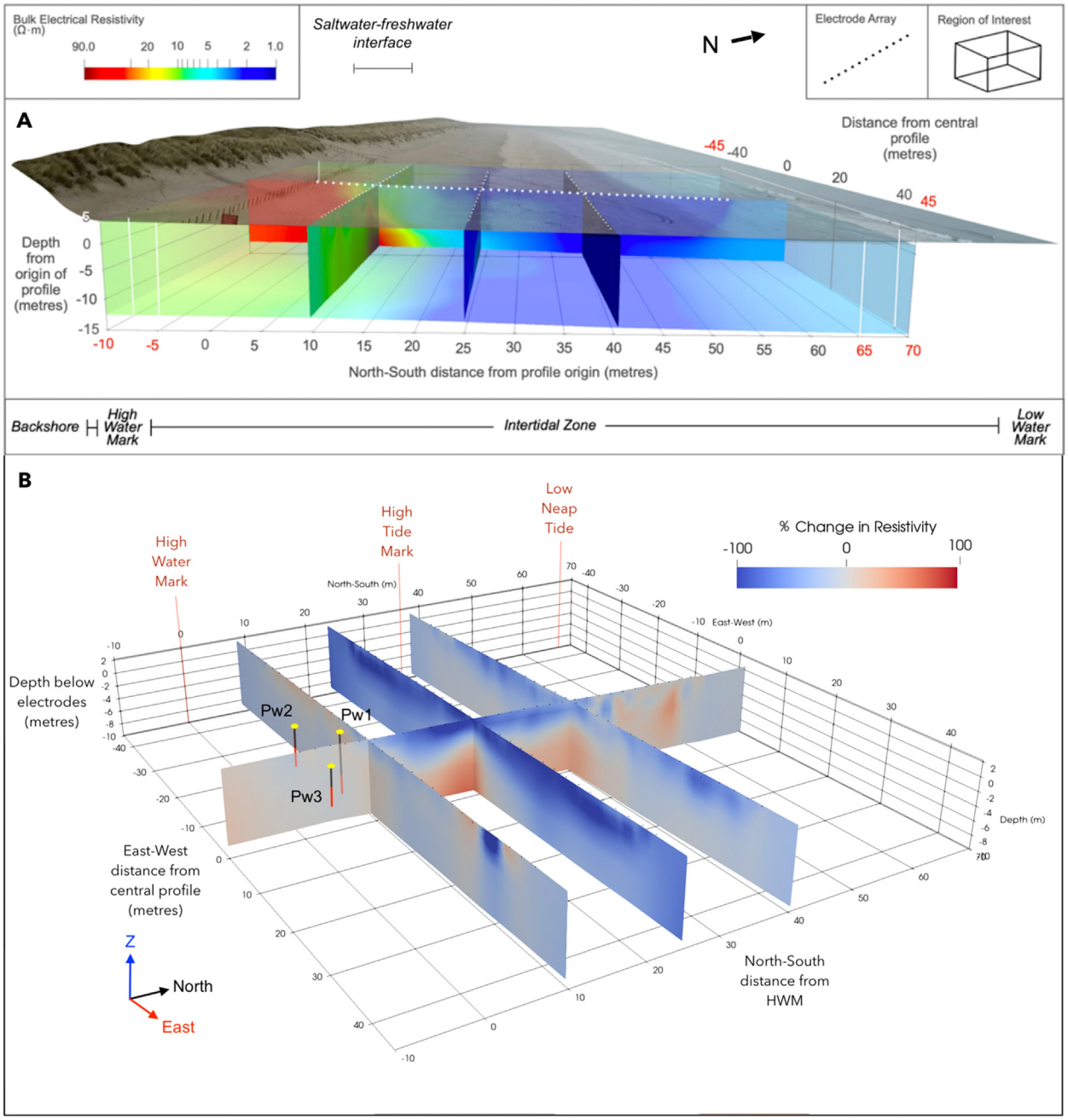

Fig. 5. (**A**) A resistivity profile from the *PRIME* array collected 10 h before the beginning of pumping at the Magilligan test site overlaid with topographical imagery of the dune, beach and sea; and (**B**) a percent-change ERI model showing the amount of change in resistivity experienced during a 28-day lunar cycle at the Magilligan test site (RMS error of the inversion: 1.98).

modeled in (Abarca et al., 2013). The north-south length of the ISC changed little over a full tidal cycle, with most change expressed at the seaward side, and almost no change at the landward side. In other words, the saltwater-freshwater interface (Fig. 5A) varies little throughout a tidal cycle. The fact there is almost no variation in resistivity in the most landward 10 m of the model contrasts with the changes in resistivity during pumping, when a net decrease in resistivity was observed. This is particularly evident around the area of the well screens, where the water was extracted. This is a strong indication that changes observed in the area around the pumping wells during pumping were not due to natural conditions.

Looking to well head chemistry as verification measure for resistivity, a consistent change in water quality is observed as pumping progresses. Using SEC as an analog for salinity, data suggest that the saltwater contribution to total discharge has increased by over 50 % during the course of pumping—with freshwater having a SEC of between 0 and 1500 μS/cm and typical sea water of about 30,000 μS/cm (Tyler et al., 2017). Conductivity initially declines in the well until reaching a minimum value of around 900 μS/cm after around 4 h of pumping. Since a lower conductivity value indicates less-saline water, this is evidence that some fresher water was drawn into the well before saline water began to intrude. The rise in DO in the pumped water is indicative of a shift to water drawn from depth at the beginning of the test, to water drawn down from nearer the surface as the pumping test progressed. The sharp step-increase in dissolved oxygen in Pw2, from approximately 2 mg/L to 8 mg/L after 23 h of pumping is unusual. Since it differs from Pw3, which is identical, a possible explanation is air leakage into the water during sample collection, as such the DO data from Pw2 could be considered unreliable. The shift in major ion water chemistry to a more NaCl dominated signature (Fig. 4) indicates

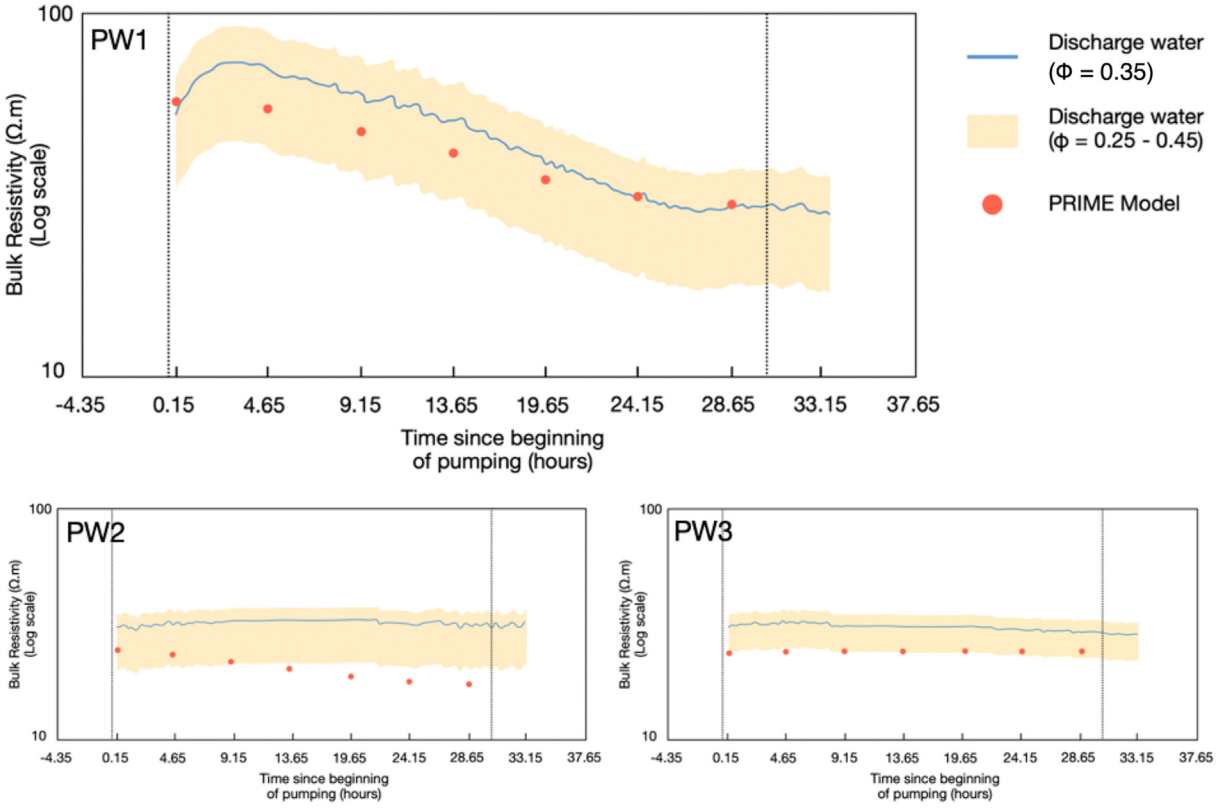

Fig. 6. Plots showing comparisons between the bulk resistivity measured and modelled by the *PRIME* system at the specific depth of abstraction in each pumping well during the pumping test at the Magilligan test site, with the bulk resistivity measured from the discharge water from each pumping well (converted from water resistivity using Archie's Law). Bulk resistivity calculations using a porosity (φ) range of 0.25 to 0.45 are also plotted (RMS error of the ERI inversion: 1.26).

that Pw1 drew in more saltwater than the other two pumping wells, as corroborated by the SEC measurements (Fig. 3C). Moreover, results of laboratory analyses reveal that Pw1 draws-in three times more saltwater than the other pumping wells. Well head chemistry data therefore indicate a clear pattern of saltwater intrusion, with the DO pattern suggesting a shallower source of saline water contributing to discharge in the latter stages of pumping.

The pumping test at Magilligan also effected a significant change in water levels relative to those observed in response to tidal fluctuations alone. Pumping wells and monitoring wells exhibited a dewatering pattern consistent with previous pumping tests at this site (McDonnell et al., 2020). Tidal fluctuations do not appear to have an effect on the rate of drawdown in this test, despite high tides coming to within 12 m of Pw1. While the observation and pumping wells reveal a pattern of dewatering, the movement of saltwater through the sand cannot be ascertained by this method alone.

Resistivity monitoring is therefore important in tracking the movement of saltwater in the subsurface. The corroboration between the bulk resistivity values of the pumped water with the bulk resistivity produced by the ERI model, using Archie's Law, indicates that the ERI system to be reliable (Fig. 6), while supporting observations that intrusion and mixing of saline and freshwater did occur across the site over the duration of pumping. The fact that the bulk resistivity values between the two sources correspond less well in Pw2 and Pw3 may be explained by their location at the very edge of the NS profile and greater distance from the EW1 profile (Fig. 1D). By contrast, Pw1 lies almost at the intersection of these two ERI lines, affording resistivity results in that region greater reliability, while the data at the very end of the NS profile suffer from lower sensitivity. This is particularly evident in the case of Pw2 which is almost 6 m away from any ERI line and displays the poorest correspondence between ERI and pumped water. This highlights the value of three-dimensional ERI layouts for more accurate representation of subsurface resistivity. The ERI array could not be positioned any further inland due to the presence of a protected habitat. The diagrams in Supplementary Material 3 displays the areas of greatest sensitivity of the PRIME system in relation to the well array.

The second validation test is the ability of the ERI to identify measurable features due to pumping – i.e., water levels in each of the wells. The data from Figs. 7 and 8 suggest that the maximum extent of dewatering (around Pw1) ranged between 2 and 6 m below ground level (including well losses). The water level measurements in Pw1 reached a maximum of 6.15 m below ground level. Two factors complicate the accurate determination of dewatering using ERI alone: the resolution of the ERI model decreases with depth; and the diffuse nature of the boundary of the area of dewatering in terms of resolution also makes it difficult to precisely define. Overall, the size of the area of dewatering represented by the ERI in Fig. 7 corresponds with the well level measurements. Since well level measurements provide data only at the locations of the wells, the dimensions of the dewatering zone produced by the ERI beyond the well field are likely to be more representative of reality than well level data. With more closely spaced electrodes, greater accuracy could be achieved at the consequence of losing information at greater depths, however it would limit the ability of the ERI to trace landward saltwater movements in the beach sands. Therefore, for the purposes of determining the suitability of a beach sand deposit to produce a reliable supply of freshwater, an ERI arrangement as utilized in this work is particularly suitable.

Since it has been established that ERI is successful at identifying patterns in groundwater salinity, it is possible to track the movement of saline water in the sand deposit using ERI, and therefore the source of the saltwater intrusion. Changes in resistivity observed during pumping in Fig. 7 indicate that the areas around the well screen depths (3–10 m below ground surface) experience a significant decline in resistivity as

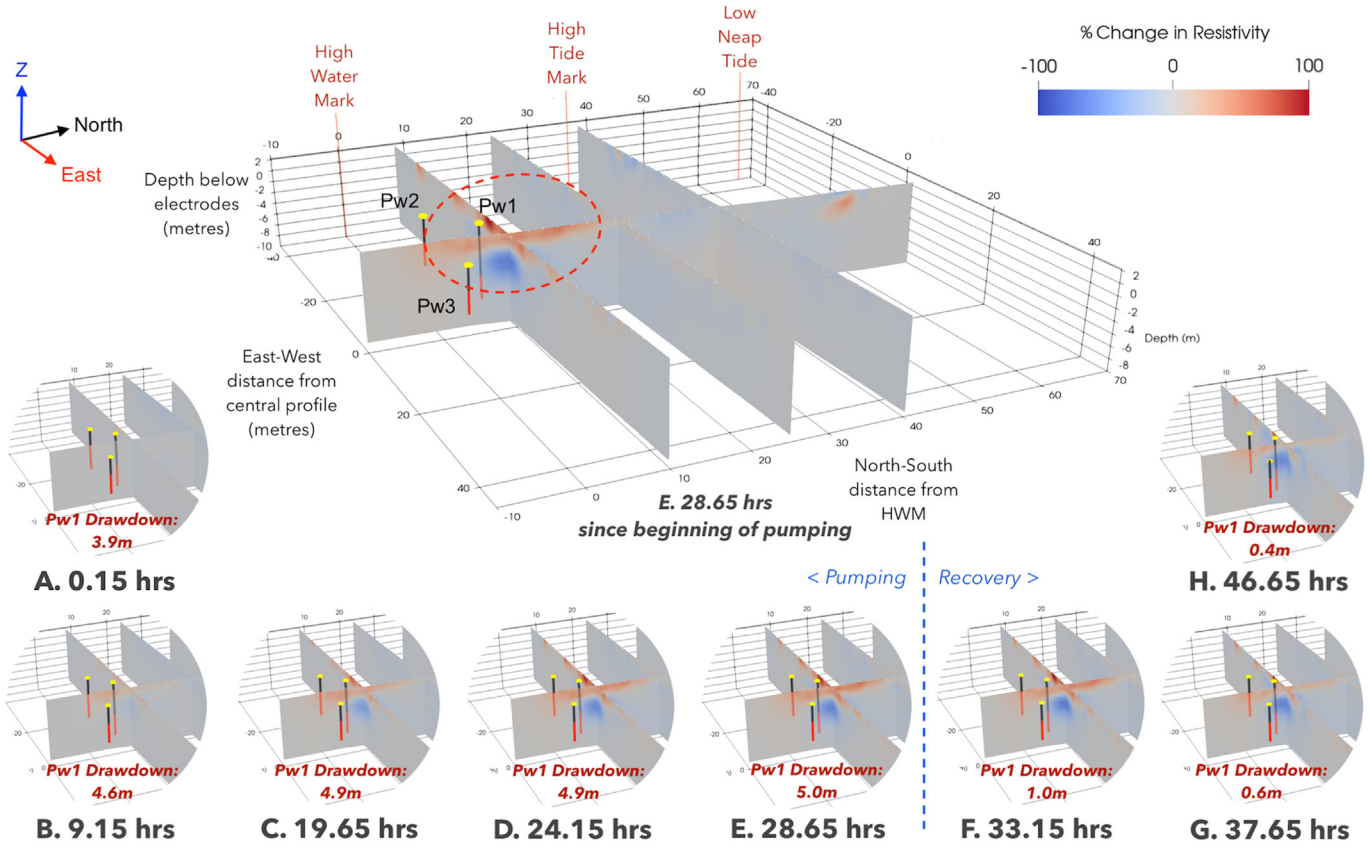

Fig. 7. Percent-change in resistivity measured at regular intervals during the pumping test at the Magilligan test site. Snapshots are identified by the time since the beginning of pumping. Those snapshots captured before and after pumping are distinguished by the blue dashed line. The location of the three pumping wells and the drawdown at Pw1 in each snapshot is displayed. Snapshot E, at the end of the pumping test, highlights the area of dewatering. Tidal markers are shown, as per Fig. 1C. The RMS error for this inversion was 1.26.

discharge water becomes more saline. The pattern of resistivity increases initially around the screened interval of Pw1 (which indicates an influx of fresh groundwater from landward of the well), before steadily decreasing until plateauing after around 27 h of pumping — which may represent the point at which only water from the ISC is being drawn into the well. It is only in Fig. 8, however, where bulk resistivity is presented in two dimensions (north-south), that movement of saltwater from the surface can be determined. The data in Fig. 8 indicate that the source of the saline content of the pumped water is derived from sources closer to the ground surface. Previous investigations by McDonnell et al. (2020) and Águila et al. (2022) have shown that the groundwater in this part of the aquifer is influenced by the surrounding saltwater, as indicated by its lowered resistivity values of around 20–30 Ω.m, when contrasted with the most landward water which is, at its highest, 148 Ω.m (Fig. 5A). This area of the sand deposit is therefore same ISC identified in, due to its position in the intertidal zone. This corroboration with the water chemistry data further strengthens the reliability of the ERI in tracking salt water movements and contributions to pumped water.

The recovery phase of pumping is only partially evident from this test due to it being followed by another test, not considered in this study. The pattern of drawdown recovery can however be extrapolated which would indicate a recovery time of 2700 min (47 h) to water levels observed prior to pumping. The ERI data reveal that the dewatered area refilled, indicated by a return to higher resistivity. It is notable that 15 h after pumping stopped, there still exists a tongue of more saline water at approximately 3-4 m below ground surface which was not present under natural pre-pumping conditions. This has implications for when the wells in this deposit, and those similar, can be pumped again following SWI. Should this beach sand deposit be considered a viable aquifer, no pumping could take place until the aquifer has returned to pre-pumping conditions. Under the pumping scenario presented here, a regime of 24 h pumping, followed by 48 h of recovery, could be considered viable.

5. Conclusions

Time-lapse ERI was applied to an unconfined coastal sand aquifer, unaffected by pumping, to characterize the source of saline intrusion induced during a pumping test. The high tidal range of over 2 m and low beach slope facilitate the formation of an extensive intertidal saline cell. Background ERI monitoring identified that over the course of one lunar cycle, the ISC waxes and wanes predominantly around the high water mark, but overall expresses little change. Pumping test instrumentation enabled the identification of dewatering in the uppermost 2 m of the sand deposit, while well head and major ion chemistry indicated a shift toward pumped water which is more saline and from a shallower source in the latter part of the test. Time-lapse ERI over the course of pumping enabled the source of saline water to be tracked and linked to the intertidal recirculation cell. Validation checks, including comparison with ERI resistivity against the resistivity of the pumped water, determined that the ERI was reliable in tracking movements of saline water. A comparison with dewatering data indicated that the ERI employed had limited precision in identifying the water table. Since the movement of saline water in this case was predominantly lateral, the ERI proved an effective tool for tracking it. Conversely findings suggested no saline intrusion via a deep basal wedge. Consequently, test findings suggest that future water resource development at the site should focus on pumping deeper parts of the aquifer. This study highlights the value of geophysical monitoring complimenting hydrogeological data. Although the instruments used are specialized and it cannot be anticipated that they be used in every scenario, the importance of reliable techniques to extract water from

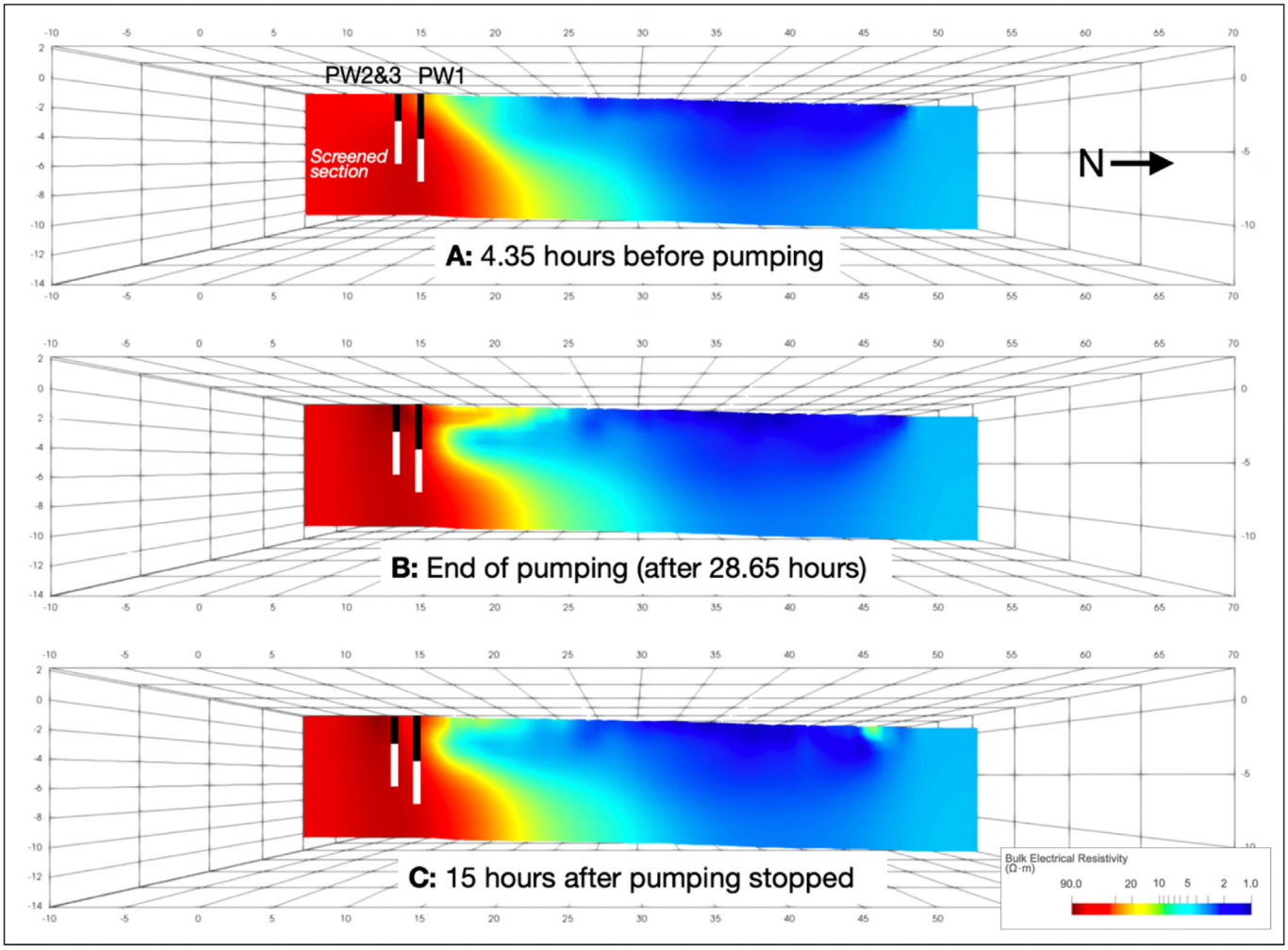

Fig. 8. North-south resistivity profiles of the sand deposit at the Magilligan aquifer 4.35 h before the pumping test began (**A**), at the end of the pumping test (after 28.65 h) (**B**), and 15 h after the pumping test had ended (**C**) Note: the landward side is to the south (left), while the seaward side is to the north (right). All snapshots are from the same north-south profile. The RMS error for this inversion was 1.26.

coastal environments will only grow in the coming decades. Through lower-cost surrogate ERI systems, temporary monitoring regimes, and the optimization of existing methods, this research paves the way for ERI to form part of a holistic approach to hydrology. This integration of water quality and geophysical data, viewed collectively to provide an improved understanding of the vulnerability of coastal aquifers, facilitates the development of measures that need to be taken to protect and develop coastal water supplies.

Supplementary data to this article can be found online at https://doi.org/10.1016/j.scitotenv.2023.161442.

CRediT authorship contribution statement

Mark C. McDonnell: Data curation, Formal analysis, Investigation, Methodology, Resources, Validation, Visualization, Writing – original draft. **Raymond Flynn:** Conceptualization, Investigation, Methodology, Project administration, Resources, Supervision, Validation, Writing – review & editing. **Jesús Fernández Águila:** Conceptualization, Data curation, Formal analysis, Investigation, Writing – review & editing. **Gerard A. Hamill:** Conceptualization, Funding acquisition, Project administration, Supervision, Writing – review & editing. **Shane Donohue:** Conceptualization, Methodology, Writing – review & editing. **Eric M. Benner:** Investigation. **Christopher Thomson:** Investigation. **Georgios Etsias:** Methodology. **Thomas S.L. Rowan:** Methodology, Investigation. **Paul B. Wilkinson:** Software. **Philip I. Meldrum:** Resources.

Data availability

Data will be made available on request.

Declaration of competing interest

The authors declare the following financial interests/personal relationships which may be considered as potential competing interests

Mark C. McDonnell reports a relationship with Queen's University Belfast that includes: funding grants and travel reimbursement

Raymond Flynn reports a relationship with Queen's University Belfast that includes: employment and travel reimbursement

Jesus Fernandez Aguila reports a relationship with Queen's University Belfast that includes: employment and travel reimbursement

Gerard A. Hamill reports a relationship with Queen's University Belfast that includes: employment and travel reimbursement

Shane Donohue reports a relationship with University College Dublin that includes: employment. Christopher Thomson reports a relationship with Queen's University Belfast that includes: funding grants

Georgios Etsias reports a relationship with Queen's University Belfast that includes: employment

Eric M. Benner reports a relationship with Queen's University Belfast that includes: employment

Paul B. Wilkinson reports a relationship with British Geological Survey that includes: employment

Philip I. Meldrum reports a relationship with British Geological Survey that includes: employment

Acknowledgements

The authors would like to thank the Ministry of Defence staff at Magilligan Training Centre for site access and support. Tidal data used in this study are from the National Tidal and Sea Level Facility, provided by the British Oceanographic Data Centre and funded by the UK Environment Agency. This work was funded by EPSRC Standard Research (Grant No. EP/R019258/1).

References

Águila, J.F., McDonnell, M.C., Flynn, R., Hamill, G.A., Ruffell, A., Benner, E.M., Etsias, G., Donohue, S., 2022. Characterizing groundwater salinity patterns in a coastal sand aquifer at Magilligan, Northern Ireland, using geophysical and geotechnical methods. Environ. Earth Sci. 81, 231. https://doi.org/10.1007/s12665-022-10357-1.

Abarca, E., Karam, H., Hemond, H.F., Harvey, C.F., 2013. Transient groundwater dynamics in a coastal aquifer: the effects of tides, the lunar cycle, and the beach profile. Water Resour. Res. 49, 2473–2488. https://doi.org/10.1002/wrcr.20075.

Archie, G.E., 1942. The electrical resistivity log as an aid in determining some reservoir characteristics. Trans. AIME 146, 54–62. https://doi.org/10.2118/942054-g.

Avachit, U., 2015. The ParaView Guide: A Parallel Visualization Application. Kitware Incorporated Paraview 4.3 ed.

Barker, R., Moore, J., 1998. The application of time-lapse electrical tomography in groundwater studies. Lead. Edge 17, 1454–1458.

Bear, J., Cheng, A.H.D., Sorek, S., Ouazar, D., Herrera, I., 1999. Seawater Intrusion in Coastal Aquifers: Concepts, Methods and Practices. Springer Netherlands 978-0-7923-5573-1.

Bevan, M.J., Endres, A.L., Rudolph, D.L., Parkin, G., 2003. The non-invasive characterization of pumping induced dewatering using ground penetrating radar. J. Hydrol. 281, 55–69.

Cardenas, M.B., Bennett, P.C., Zamora, P.B., Befus, K.M., Rodolfo, R.S., Cabria, H.B., Lapus, M.R., 2015. Devastation of aquifers from tsunami-like storm surge by Supertyphoon Haiyan. Geophys. Res. Lett. 42, 2844–2851. https://doi.org/10.1002/2015GL063418.

Carter, R.W.G., 1975. Recent Changes in the Coastal Geomorphology of the Magilligan Foreland, Co. Londonderry. 75. Royal Irish Academy of Chemical Science, pp. 469–497.

Chambers, J.E., Gunn, D.A., Wilkinson, P.B., Meldrum, P.I., Haslam, E., Holyoake, S., Kirkham, M., Juras, O., Merritt, A., Wragg, J., 2014. 4D electrical resistivity tomography monitoring of soil moisture dynamics in an operational railway embankment. Near Surf. Geophys. 12, 61–72. https://doi.org/10.3997/1873-0604.2013002.

Chang, P.Y., Chang, L.C., Hsu, S.Y., Tsai, J.P., Chen, W.F., 2017. Estimating the hydrogeological parameters of an unconfined aquifer with the time-lapse resistivity-imaging method during pumping tests: case studies at the Pengtsuo and Dajou sites, Taiwan. J. Appl. Geophys. 144, 134–143. https://doi.org/10.1016/j.jappgeo.2017.06.014.

Endres, A.L., Clement, W.P., Rudolph, D.L., 2000. Ground penetrating radar imaging of an aquifer during a pumping test. Ground Water 38, 566–576.

Freeze, R.A., Cherry, J.A., 1979. Groundwater. Prentice-Hall, Englewood Cliffs, NJ doi:ISBN: 0-13-365312-9.

Hermans, T., Paepen, M., 2020. Combined inversion of land and marine electrical resistivity tomography for submarine groundwater discharge and saltwater intrusion characterization. Geophys. Res. Lett. 47 (3). https://doi.org/10.1029/2019gl085877.

Holmes, J., Chambers, J., Meldrum, P., Wilkinson, P., Boyd, J., Williamson, P., Huntley, D., et al., 2020. Four-dimensional electrical resistivity tomography for continuous, near-real-time monitoring of a landslide affecting transport infrastructure in British Columbia, Canada. Near Surf. Geophys. (Wiley) 18 (4), 337–351 (Wiley).

Holmes, J., Chambers, J., Wilkinson, P., Dashwood, B., Gunn, D., Cimpoiaşu, M., Kirkham, M., et al., 2022. 4D electrical resistivity tomography for assessing the influence of vegetation and subsurface moisture on railway cutting condition. Eng. Geol. 307, 106790. https://doi.org/10.1016/j.enggeo.2022.106790.

Johnson, T.C., Versteeg, R.J., Ward, A., Day-Lewis, F.D., Revil, A., 2010. Improved hydrogeophysical characterization and monitoring through high performance electrical geophysical modeling and inversion. Geophysics 75 (4), WA27–WA41. https://doi.org/10.1190/1.3475513.

LaBrecque, D.J., Heath, G., Sharpe, R., Versteeg, R., 2004. Autonomous monitoring of fluid movement using 3-D electrical resistivity tomography. J. Environ. Eng. Geophys. 9 (3), 167–176.

Land, L.A., Lautier, J.C., Wilson, N.C., Chianese, G., Webb, S., 2004. Geophysical monitoring and evaluation of coastal plain aquifers. Ground Water 42, 59–67.

Legaz, A., Vandemeulebrouck, J., Revil, A., Kemna, A., Hurst, A.W., Reeves, R., Papasin, R., 2009. A case study of resistivity and self-potential signatures of hydrothermal instabilities, Inferno Crater Lake, Waimangu, New Zealand. Geophys. Res. Lett. 36, L12306.

Loke, M.H., 2022. 2-D and 3-D Electrical Imaging Surveys. Geotomo Software Tutorial.

Loke, M.H., 2017. RES3DINVx64 ver. 4.07 with multi-core and 64-bit support for Windows XP/Vista/7/8/10. Rapid 3-D Resisitivity & IP inversion using the least-squares method. Geoelectrical Imaging 2-D and 3-D. Geotomo Software.

Loke, M.H., Barker, R.D., 1995. Least-squares deconvolution of apparent resistivity pseudosections. Geophysics 60, 1682–1690.

Loke, M.H., Barker, R.D., 1996. Rapid least-squares inversion of apparent resistivity pseudosections by a quasi-Newton method. Geophys. Prospect., 131–152 https://doi.org/10.1111/j.1365-2478.1996.tb00142.x.

Müller, K., Vanderborght, J., Englert, A., Kemna, A., Huisman, J.A., Rings, J., Vereecken, H., 2010. Imaging and characterization of solute transport during two tracer tests in a shallow aquifer using electrical resistivity tomography and multilevel groundwater samplers. Water Resour. Res. 46, W03502. https://doi.org/10.1029/2008WR007595.

Maury, S., Balaji, S., 2015. Application of resistivity and GPR techniques for the characterization of the coastal litho-stratigraphy and quifer vulnerability due to seawater intrusion. Estuar. Coast. Shelf Sci. 104–116.

McCann, N., 1988. An assessment of the subsurface geology between Magilligan point and fair head, Northern Ireland. Ir.J.Earth Sci. 9, 71–78.

McDonnell, M.C., Águila, J.F., Flynn, R., Hamill, G., Etsias, G., Benner, E., 2020. Water Extraction From Coastal Sand Aquifers in Ireland: An Extreme Case at Magilligan, County Derry. Civil Engineering Research in Ireland, Cork, Ireland. ISBN: 978-09573957-4-9, pp. 726–731.

Ogilvy, R., Meldrum, P., Kuras, O., Wilkinson, P., Chambers, J., Sen, M., Pulido-Bosch, A., et al., 2009. Automated monitoring of coastal aquifers with electrical resistivity tomography. Near Surf.Geophys. 7, 367–376. https://doi.org/10.3997/1873-0604.2009027.

Pidlisecky, A., Knight, R., 2008. FW2_5D: A MATLAB 2.5-D electrical resistivity modeling code. Comput. Geosci. 34 (12), 1645–1654.

Pidlisecky, A., Haber, E., Knight, R., 2007. RESINVM3D: a 3D resistivity inversion package. Geophysics 72 (2), H1–H10.

Pingree, R.D., Griffiths, D.K., 1981. Sand transport paths around the British Isles resulting from M2 and M4 tidal interactions. J. Mar. Biol. Assoc. U. K. 59 (2), 497–513.

Pollock, D., Cirpka, O.A., 2012. Fully coupled hydrogeophysical inversion of a laboratory salt tracer experiment monitored by electrical resistivity tomography. Water Resour. Res. 48, W01505. https://doi.org/10.1029/2011WR010779.

Rizzo, E., Suski, B., Revil, A., Straface, S., Troisi, S., 2004. Self-potential signals associated with pumping tests experiments. J. Geophys. Res. (Am. Geophys. Union) 109 (B10). https://doi.org/10.1029/2004JB003049.

Robins, N.S., Wilson, P., 2017. A conceptual snapsot of a big coastal dune aquifer: Magilligan, Northern Ireland. J. Coast. Conserv. 21, 615–621. https://doi.org/10.1007/s11852-017-0503-y.

Straface, S., Troisi, C., Falico, S., Rizzo, E., Revil, A., 2007. Estimating of the transmissivities of a real aquifer using self potential signals associated with a pumping test. Ground Water 45 (4), 420–428.

Tyler, R.H., Boyer, T.P., Minami, T., Zweng, M.M., Reagan, J.R., 2017. Electrical conductivity of the global ocean. Earth, Planets and Space 69 (1) (Springer Science and Business Media LLC.).

Uhlemann, S., Chambers, J., Wilkinson, P., Maurer, H., Merritt, A., Meldrum, P., Kuras, O., Gunn, D., Smith, A., Dijkstra, T., 2017. Four-dimensionalimaging of moisture dynamics duringlandslide reactivation. J. Geophys. Res. 122, 398–418. https://doi.org/10.1002/2016JF003983.

Werner, A.D., Bakker, M., Post, V.E.A., Vandenbohede, A., Lu, C., Ataie-Ashtiani, B., Simmons, C.T., Barry, D.A., 2013. Seawater intrusion processes, investigation and management: Recent advances and future challenges. Adv. Water Resour. 51, 3–26. https://doi.org/10.1016/j.advwatres.2012.03.004 (Elsevier BV.).

Zarroca, M., Bach, J., Linares, R., Pellicer, X.M., 2011. Electrical methods (VES and ERT) for identifying, mapping and monitoring different saline domains in a coastal plain region (Alt Emporada, Northern Spain). J. Hydrol. 409, 401–422.